

Realize high thermoelectric performance in both zone-melted ingots and powder-metallurgy bulks of $Bi_{0.46}Sb_{1.54}Te_3$

Kai-Wen Zhao(赵凯雯), Meng-Yao Li(李梦瑶), Ying-Jiu Zhang(张迎九), and Hong-Zhang Song(宋红章)

Citation: Chin. Phys. B, 2025, 34 (**10**): 107203. DOI: 10.1088/1674-1056/add503
http://cpb.iphy.ac.cn; http://iopscience.iop.org/cpb

What follows is a list of articles you may be interested in

High thermoelectric performance of SnS under high pressure and high temperature

Yuqi Gao(高语崎), Xinglin Wang(王星淋), Cun You(由存), Dianzhen Wang(王殿振), Nan Gao(高楠), Qi Jia(贾琪), Zhihui Li(李志慧), Qiang Tao(陶强), and Pinwen Zhu(朱品文)

Chin. Phys. B, 2025, 34 (**8**): 087201. DOI: 10.1088/1674-1056/addbc8

High-entropy alloys in thermoelectric application: A selective review

Kai Ren(任凯), Wenyi Huo(霍文燚), Shuai Chen(陈帅), Yuan Cheng(程渊), Biao Wang(王彪), and Gang Zhang(张刚)

Chin. Phys. B, 2024, 33 (**5**): 057202. DOI: 10.1088/1674-1056/ad34c5

Rational design and synthesis of $Cr_{1-x}Te/Ag_2Te$ composites for solid-state thermoelectromagnetic cooling near room temperature

Xiaochen Sun(孙笑晨), Chenghao Xie(谢承昊), Sihan Chen(陈思汗), Jingwei Wan(万京伟), Gangjian Tan(谭刚健), and Xinfeng Tang(唐新峰)

Chin. Phys. B, 2024, 33 (**5**): 057201. DOI: 10.1088/1674-1056/ad2d57

Ga intercalation in van der Waals layers for advancing p-type Bi_2Te_3-based thermoelectrics

Yiyuan Chen(陈艺源), Qing Shi(石青), Yan Zhong(钟艳), Ruiheng Li(李瑞恒), Liwei Lin(林黎蔚), Ding Ren(任丁), Bo Liu(刘波), and Ran Ang(昂然)

Chin. Phys. B, 2023, 32 (**6**): 067201. DOI: 10.1088/1674-1056/acc2af

Advancing thermoelectrics by suppressing deep-level defects in Pb-doped $AgCrSe_2$ alloys

Yadong Wang(王亚东), Fujie Zhang(张富界), Xuri Rao(饶旭日), Haoran Feng(冯皓然), Liwei Lin(林黎蔚), Ding Ren(任丁), Bo Liu(刘波), and Ran Ang(昂然)

Chin. Phys. B, 2023, 32 (**4**): 047202. DOI: 10.1088/1674-1056/acb765

Realize high thermoelectric performance in both zone-melted ingots and powder-metallurgy bulks of $Bi_{0.46}Sb_{1.54}Te_3$

Kai-Wen Zhao(赵凯雯), Meng-Yao Li(李梦瑶)[†], Ying-Jiu Zhang(张迎九), and Hong-Zhang Song(宋红章)[‡]

Key Laboratory of Materials Physics of the Ministry of Education, School of Physics and Laboratory of Zhongyuan Light, Zhengzhou University, Zhengzhou 450001, *China*

(Received 19 March 2025; revised manuscript received 25 April 2025; accepted manuscript online 7 May 2025)

$Bi(Sb)_2Te(Se)_3$ alloys, as the only commercial thermoelectric materials, have been applied widely in cooling fields. While, the current energy conversion efficiency (dominated by the dimensionless *ZT*) of commercial products is still lower and cannot meet the market demand. In this paper, high thermoelectric performance at room temperature in both zone-melted (ZM) $Bi_{0.46}Sb_{1.54}Te_3$ ingots and powder-metallurgy (PM) $Bi_{0.46}Sb_{1.54}Te_3$ blocks with a large size was realized successfully by optimizing their preparation process. The peak *ZT* values of ZM and PM p-type $Bi_{0.46}Sb_{1.54}Te_3$ alloys reached 1.26 and 1.45, respectively. They are higher than those of all the n-type or p-type Bi_2Te_3-based products in current commercial applications. In particular, their production process of large size p-type $Bi_{0.46}Sb_{1.54}Te_3$ alloys could be directly industrialized.

Keywords: thermoelectric, $Bi_{0.46}Sb_{1.54}Te_3$, large size

PACS: 72.15.Jf, 81.20.Ev

DOI: 10.1088/1674-1056/add503 **CSTR:** 32038.14.CPB.add503

1. Introduction

At present, the serious energy crisis and environmental problems have aroused widespread concern on exploring sustainable and eco-friendly energy resources.[1,2] Thermoelectric devices can converse directly electricity and heat with many advantages.[3–5] The performance of thermoelectric materials is typically assessed by the dimensionless thermoelectric figure of merit (*ZT*, $ZT = \frac{S^2\sigma}{\kappa_t}T$),[6–11] where κ_t is the total thermal conductivity, *S* is the Seebeck coefficient, σ is the electrical conductivity, and *T* is the absolute temperature. Therefore, excellent thermoelectric materials must have low κ_t and high power factors ($PF = S^2\sigma$) simultaneously. Their optimized strategies include energy band engineering,[12–16] and phonons engineering,[17–29] etc.

Currently, Bi_2Te_3-based thermoelectric alloys dominate the room temperature thermoelectric cooling (TEC) devices due to their excellent thermal and electrical stabilities.[30–33] On the one hand, the zone-melting (ZM) method is commonly used to produce commercial bismuth telluride. However, *ZT* values of p-type zone-melted Bi_2Te_3 ingots is low,[34] and needs further improvement. On the other hand, the poor mechanical strengths of such ingots limit the application in miniature devices. The processability and mechanical strengths can be optimized by the powder-sintering or powder-metallurgy (PM) method.[35,36] Currently, polycrystalline Bi_2Te_3-based thermoelectric alloys prepared by PM can be cut into small π-legs with a cross-section of 0.1 mm × 0.1 mm, but their thermoelectric performance needs further improvement too.[37–40]

In our previous work, high thermoelectric performance was achieved successfully in large size n-type $Bi_2Te_{2.7}Se_{0.3}$ ingots.[41] Further, high thermoelectric and mechanical properties were realized in n-type $Bi_2Te_{2.7}Se_{0.3}$ bulks through PM and carrier concentration regulation.[37,42] TEC devices need both n-type and p-type Bi_2Te_3-based π-legs. In this paper, high thermoelectric properties of large size p-type $Bi_{0.46}Sb_{1.54}Te_3$ ingots were realized by optimizing the preparation conditions, and their large size polycrystalline bulks were obtained by further PM. Finally, the *ZT* of the samples prepared by the ZM method reached a peak value of 1.26 at 360 K along the ZM growth direction. The $Bi_{0.46}Sb_{1.54}Te_3$ PM bulks have the peak *ZT* value (ZT_{max}) of 1.45 at 300 K.

2. Experimental details

The large size p-type $Bi_{0.46}Sb_{1.54}Te_3$ ingots (length in 300 mm, diameter in 30 mm) were prepared by the ZM method. The process was similar to our earlier work of n-type $Bi_2Te_{2.7}Te_{0.3}$ ingots.[34] The large size p-type $Bi_{0.46}Sb_{1.54}Te_3$ polycrystalline bulks (30 mm × 30 mm × 70 mm) were prepared by the ZM, pulverizing, grinding, and vacuum hot-pressing (HP) method. The process was similar to our previous work of n-type $Bi_2Te_{2.7}Te_{0.3}$ polycrystalline bulks.[36,42] The ingots and polycrystalline bulks were cut into 2 mm × 4 mm × 13 mm for electrical property testing, and 2 mm × 10 mm × 10 mm for thermal performance testing. Regarding to the anisotropy, the ZM∥ meant the testing direction parallel to the ZM growth

[†]Corresponding author. E-mail: limengyaorz@zzu.edu.cn

[‡]Corresponding author. E-mail: hzsong@zzu.edu.cn

© 2025 Chinese Physical Society and IOP Publishing Ltd. All rights, including for text and data mining, AI training, and similar technologies, are reserved.

direction, and the ZM⊥ meant the testing direction perpendicular to the ZM growth direction. The testing direction of polycrystalline bulks was perpendicular to the pressure.

The microstructure was observed by the scanning electron microscope (SEM, JSM-6700F). The Seebeck coefficient and electrical resistivity were simultaneously measured using the LSR-3/800 system (Linseis, Germany) under helium atmosphere. An error of approximately 4% in the measurement of both electrical conductivity and the Seebeck coefficient was estimated. The thermal diffusivity D was measured by using the FLASHLINE^{TM}3000 (ANTER, USA) and the LFA-457 (Netzsch, Germany), the estimated error of approximately 5%. The total thermal conductivity κ_t ($\kappa_t = D\rho C_p$) was calculated by measuring the specific heat C_p, thermal diffusivity D, and density ρ. The Hall carrier concentration and mobility were measured at room temperature using the Van der Pauw method under 0.5-T magnetic field conditions with an estimated error of approximately 10% (HMS-5500, ECOPIA, Korea).

3. Results and discussion

As illustrated in Fig. 1, the XRD pattern of the powder obtained by crushing and sieving the sample prepared by ZM is shown. The diffraction peaks in the image are consistent with the PDF card, demonstrating a single-phase rhombohedral structure. This indicates that the prepared sample is pure $Bi_{0.46}Sb_{1.54}Te_3$. Both large size ZM ingots and HP bulks of $Bi_{0.46}Sb_{1.54}Te_3$ are prepared successfully, and their macroscopic photographs are shown in Fig. 2(a). In order to further observe the internal topography of samples, the fracture surface was characterized by the SEM, as shown in Figs. 2(b)–2(d). The fracture surface morphologies of the samples prepared by zone-melting method along the crystal growth direction (ZM∥) and vertical crystal growth direction (ZM⊥) are shown in Figs. 2(b) and 2(c), respectively. The crystal plane size along the grain growth direction (ZM∥) is very larger. The fracture surface in vertical growth direction exhibits an obvious orientation and layered structure, and the grain size is larger. They demonstrate an excellent ZM growth. Due to the obvious difference in the microscopic morphology of the two directions, the thermoelectric properties of the two directions are also significantly different, which can also be obviously observed in the subsequent thermoelectric performance images. Figure 2(d) shows the fracture surface of the HP sample, which exhibits typical polycrystalline structure. Many grain boundaries are introduced, and the grain size of the HP sample is significantly reduced. While, the layered structure of the bismuth telluride-based sample can still be observed, which is similar to the results of previous literatures.[36]

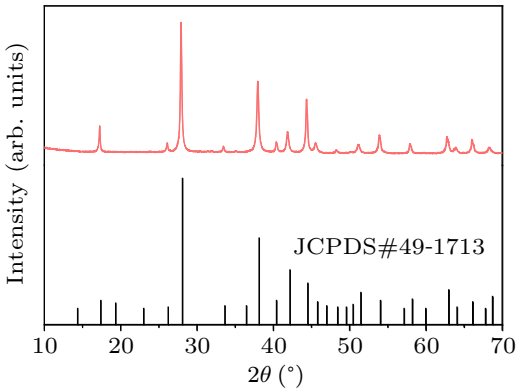


Fig. 1. XRD patterns of the $Bi_{0.46}Sb_{1.54}Te_3$ powder.

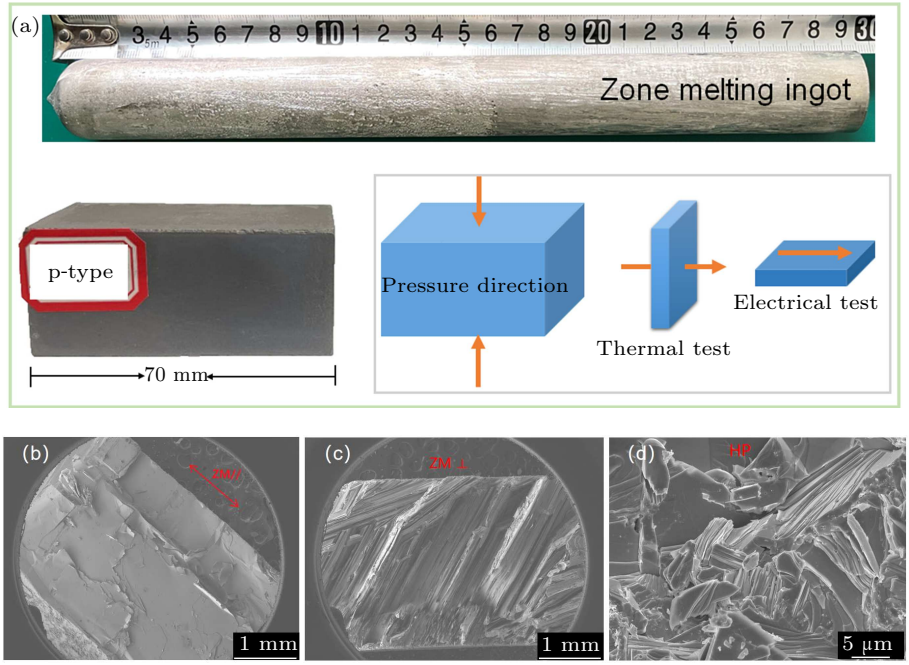


Fig. 2. (a) Macroscopic photographs of ZM and HP $Bi_{0.46}Sb_{1.54}Te_3$ samples and schematic measuring illustration, (b)–(d) SEM fracture surface images of (ZM∥), (ZM⊥), and HP.

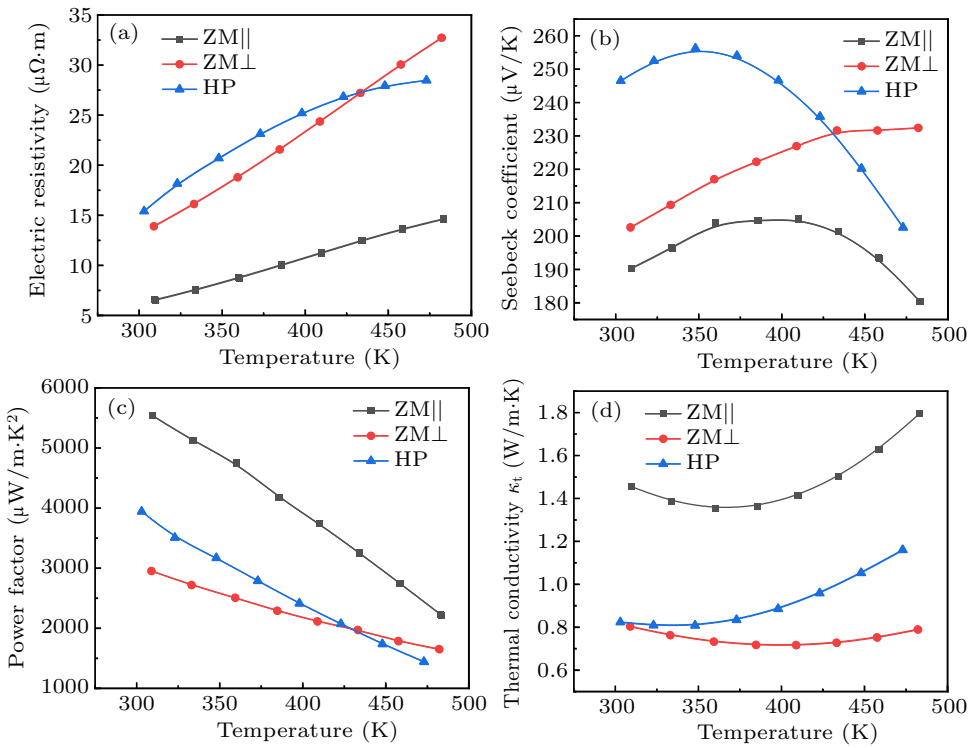


Fig. 3. Thermoelectric transport properties of zone-melted and hot-pressed $Bi_{0.46}Sb_{1.54}Te_3$ samples: (a) electrical resistivity ρ, (b) Seebeck coefficient S, (c) power factor PF, (d) thermal conductivity κ_t.

Figures 3(a)–3(d) display the electrical resistivity, power factor, Seebeck coefficient, and thermal conductivity as functions of temperature for ZM and HP $Bi_{0.46}Sb_{1.54}Te_3$ samples. In Fig. 3(a), the electrical resistivity of all samples increases gradually with the increase of temperature, demonstrating metal-conducting behavior, and their degenerate semiconductor nature, which obeys the common characteristic of Bi_2Te_3-based materials. Among them, the resistivity in two ZM directions is very different, such as at room temperature, the resistivity of the ZM$\parallel$ sample is 6.5 μΩ·m, and the resistivity of the ZM$\perp$ sample is 13.8 μΩ·m. The difference between the two is nearly 53%, exhibiting strong anisotropy. The resistivity perpendicular to the zone growth direction is high, which is attributed to the enhanced carrier scattering by layered grains. The HP sample has relatively high resistivity. On the one hand, the HP causes the donor-like effect, thus reduces the carrier concentration.[43,44] On the other hand, the polycrystalline grain boundary enhances the carrier scattering, thus reduces the carrier mobility. Their carrier concentrations are 7.06×10^{19} cm^{-3}, 5.27×10^{19} cm^{-3}, 2.71×10^{19} cm^{-3}. Their carrier mobilities are 897.7 cm^2·V^{-1}·s^{-1}, 107.6 cm^2·V^{-1}·s^{-1}, 188.8 cm^2·V^{-1}·s^{-1} for ZM$\parallel$, ZM$\perp$, and HP samples, respectively. These Hall test results are also in agreement with the results of resistivity.

Figure 3(b) shows the Seebeck curves with temperature change. The positive Seebeck coefficients of all samples indicate that the major carriers in the samples are holes, which is consistent with the characteristics of p-type $Bi_{0.46}Sb_{1.54}Te_3$ materials. It can be clearly seen that the Seebeck coefficients of the HP sample are large. The Seebeck coefficients of the samples obtained by ZM are still different in two directions, and the ZM$\perp$ Seebeck coefficient is relatively large at higher temperature. This phenomenon is attributed to the intrinsic excitation, which is consistent with references.[45,46]

The curve of power factor (PF) variation with temperature calculated by the Seebeck coefficient and resistivity is shown in Fig. 3(c). Because the very low resistivity of the sample parallel to the ZM direction compensates for the slightly lower Seebeck coefficient in this direction, the power factor obtained parallel to the zone-melting direction is the highest, reaching 5540 μW/m·K^2 at room temperature. Compared with reported literatures of Bi_2Te_3-based materials,[37,38,41–43,47–49] this PF value is one of the highest, meaning an excellent thermoelectric power. It is 47% higher than that in the vertical direction, and is 29% higher than that of the HP sample.

Figure 3(d) shows the thermal conductivity curve of the materials with temperature. All the thermal conductivity increases at high temperature, mainly due to the contribution of additional bipolar diffusion thermal conductivity, which accords with the narrow bandgap characteristic of bismuth telluride-based thermoelectric materials. The thermal conductivity in different directions is obviously different. The ZM$\parallel$ sample has the highest thermal conductivity due to weakened phonon scattering. The lower thermal conductivity of the samples prepared by the HP method is mainly due to the fact that the polycrystals of the samples prepared by this method have more crystalline boundary or interfaces as compared to the samples prepared by the ZM method, which will favour the

scattering of phonons within the material and thus reduce the thermal conductivity.

Figure 4(a) demonstrates the temperature dependence of ZT of ZM and HP $Bi_{0.46}Sb_{1.54}Te_3$ samples. The ZT value of the HP sample is higher at low temperature, and reaches a peak value of 1.45 at 300 K. This ZT_{max} value in this work exceeds those of most reported p-type BiSbTe-based materials. The ZT of the ZM sample along the growth direction reaches a peak value of 1.26 at 360 K. Although it is lower than that of the HP sample, it is an excellent result in reported ZM ingots. Figures 4(b) and 4(c) summarize and compare some advanced ZT values of p-type Bi_2Te_3-based thermoelectric materials over the last decade along with the years.[44,49–66] It can be seen that at room temperature, the HP sample in this work exhibits a higher level, which is beneficial for the TEC application of Bi_2Te_3-based thermoelectric materials.

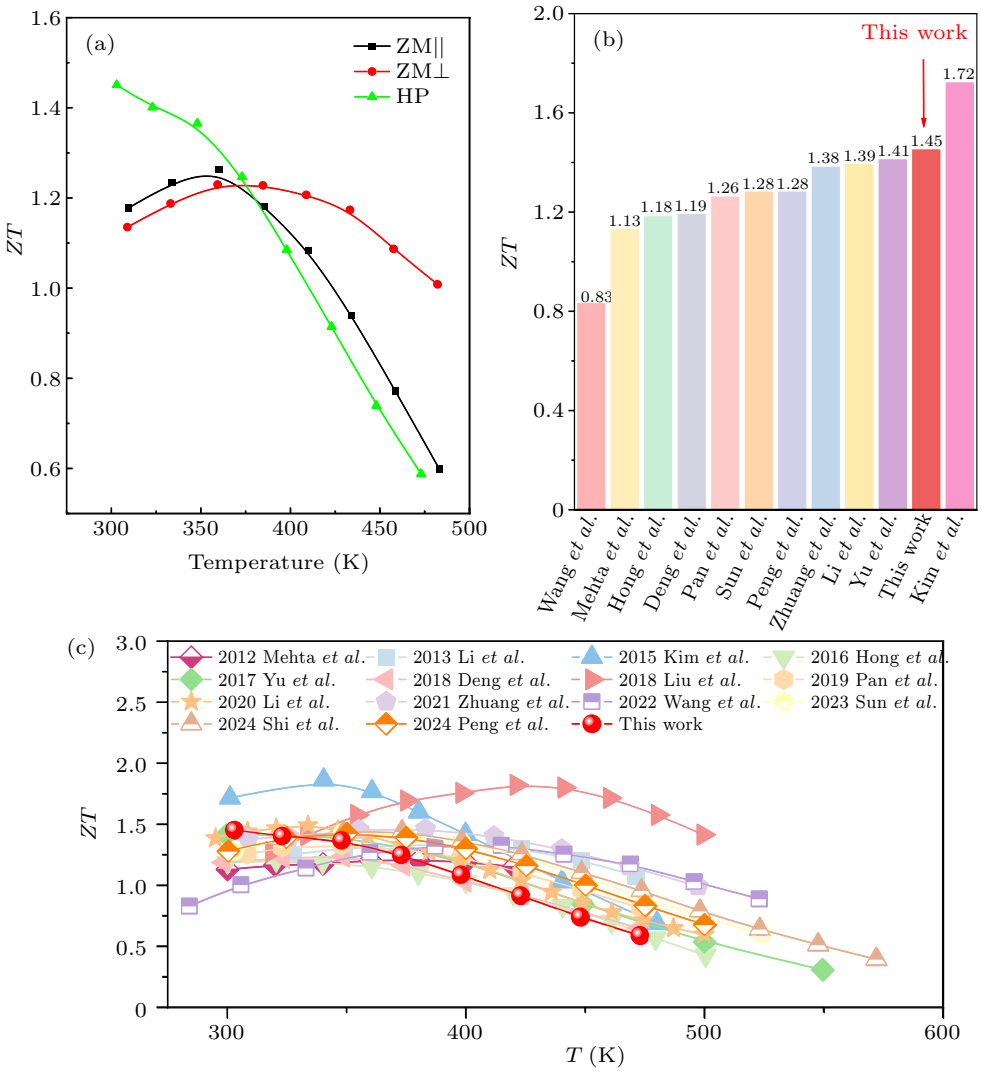


Fig. 4. (a) The ZT curves of ZM and HP $Bi_{0.46}Sb_{1.54}Te_3$ samples, (b) reported ZT values in BiSbTe-based materials at room temperature, (c) reported ZT curves in BiSbTe-based materials.

4. Conclusions

On the one hand, by optimizing the ZM preparation process, the large size $Bi_{0.46}Sb_{1.54}Te_3$ ingot achieves an excellent thermoelectric performance, its ZT_{max} reaches 1.26 at 360 K. This value is higher than those of all the current n-type or p-type Bi_2Te_3-based ingots in commercial applications. On the other hand, by combining optimized ZM, BM, and HP, large size $Bi_{0.46}Sb_{1.54}Te_3$ polycrystalline bulks weaken the anisotropy, enhance the mechanical strengths of ZM ingots, and realize high thermoelectric performance with a ZT_{max} of 1.45 at 300 K. This production process of large size p-type $Bi_{0.46}Sb_{1.54}Te_3$ polycrystalline bulks could be directly industrialized, targeting the TEC devices.

Acknowledgements

Project supported by the National Key Research and Development Program of China (Grant No. 2024YFE0105200), the China Postdoctoral Science Foundation (Grant No. 2023M743151), and the Natural Science Foundation of Henan Province, China (Grant No. 242300420304).

References

[1] Dai S, Lin Z, Hu H, Wang Y and Zeng L 2024 *Appl. Phys. Rev.* **11** 041319
[2] Li X, Zhang X, Xu J, Duan Z, Xu Y, Zhang X, Zhang L, Wang Y and Chu P K 2024 *Adv. Sci.* **11** 2305467
[3] Qin Y, Qin B, Hong T, Zhang X, Wang D, Liu D, Wang Z Y, Su L, Wang S and Gao X 2024 *Science* **383** 1204
[4] Chen W Y, Shi X L, Zou J and Chen Z G 2022 *Mater. Sci. Eng. R: Rep.* **151** 100700
[5] Deng T, Gao Z, Li Z, Qiu P, Li Z, Yuan X, Ming C, Wei T R, Chen L and Shi X 2024 *Science* **386** 1112
[6] Hu H, Ju Y, Yu J, Wang Z, Pei J, Thong H C, Li J W, Cai B, Liu F and Han Z 2024 *Nat. Mater.* **23** 527
[7] Tian Q, Zhang W, Qin Z and Qin G 2021 *Nanoscale* **13** 18032
[8] Zhou Z, Huang Y, Wei B, Yang Y, Yu D, Zheng Y, He D, Zhang W, Zou M and Lan J L 2023 *Nat. Commun.* **14** 2410
[9] Lei J, Wuliji H, Ren Q, Hao X, Dong H, Chen H, Wei T R, Zhang J, Qiu P and Zhao K 2024 *Energy & Environmental Science* **17** 1416
[10] Zhu Y, Wan B, Shen W, Zhang Z, Fang C, Wang Q, Chen L, Zhang Y and Jia X 2023 *Appl. Phys. Lett.* **122** 133903
[11] Tian Q, Li P, Wei J, Xing Z, Qin G and Qin Z 2023 *Phys. Rev. B* **108** 115130
[12] Liu S, Bai S, Wen Y, Lou J, Jiang Y, Zhu Y, Liu D, Li Y, Shi H and Liu S 2025 *Science* **387** 202
[13] Shi X, Song S, Gao G and Ren Z 2024 *Science* **384** 757
[14] Wu B, Zhao X, Jia M, Yang D, Liu Y, Song H, Wang D, Cabot A and Li M 2024 *Appl. Phys. Lett.* **125** 223901
[15] Zhu Z, Zhang Y, Song H and Li X J 2018 *Appl. Phys. A* **124** 871
[16] Zhu Z, Zhang Y, Song H and Li X J 2018 *Appl. Phys. A* **124** 747
[17] Yang S, Ming H, Li D, Chen T, Li S, Zhang J, Xin H and Qin X 2023 *Chem. Eng. J.* **455** 140923
[18] Xu Y, Xia S, Zhang Y, Song H, Liu S and Hao H 2024 *Appl. Phys. A* **130** 203
[19] Ma R, Yang D, Li X, Song H and Zhang Y 2022 *Appl. Phys. A* **128** 1134
[20] Ma R, Yang D, Tian Z, Song H and Zhang Y 2022 *Appl. Phys. A* **128** 531
[21] Zhu Z, Zhang Y, Song H and Li X J 2019 *Appl. Phys. A* **125** 572
[22] Cao R, Li E, Hu Q, Zhu Z, Zhang Y, Li X, Hu X and Song H 2018 *Appl. Phys. A* **124** 669
[23] Xue T, Wei P, Liu C, Li L, Zhu W, Nie X and Zhao W 2024 *Chin. Phys. B* **33** 087403
[24] Ren K, Huo W, Chen S, Cheng Y, Wang B and Zhang G 2024 *Chin. Phys. B* **33** 057202
[25] He Q, Yang D, Zhang W and Song H 2024 *Mod. Phys. Lett. B* **38** 2450224
[26] He Q, Zhang W, Liu X and Song H 2022 *Mod. Phys. Lett. B* **36** 2250157
[27] Zhang Y, Fan M M, Ruan C C, Zhang Y W, Li X J and Song H Z 2020 *Mod. Phys. Lett. B* **34** 2050019
[28] Li S, Wang L, Ma D, Jiang Y, Zhang J and Guo K 2024 *ACS Appl. Mater. Interfaces* **16** 3586
[29] Li S, Zhao W, Cheng Y, Chen L, Xu M, Guo K and Pan F 2022 *ACS Appl. Mater. Interfaces* **15** 1167
[30] Liu Q, Lu Y, Zhu H, Qian X, Yang R and Zhao H 2024 *Sci. Bull.* **69** 295
[31] Yen W T, Wang K K and Wu H J 2023 *Materials Today Physics* **34** 101065
[32] Zhang X, Wang Z, Hou Y, Liu Y, Hu L, Xie W, Shi J, Wei J and Xiong R 2024 *Chem. Eng. J.* **481** 148530
[33] Zheng Y, Tan X Y, Wan X, Cheng X, Liu Z and Yan Q 2019 *ACS Appl. Energy Mater.* **3** 2078
[34] Zhu T, Liu Y, Fu C, Heremans J P, Snyder J G and Zhao X 2017 *Adv. Mater.* **29** 1605884
[35] Pan Y, Wei T R, Cao Q and Li J F 2015 *Mater. Sci. Eng. B* **197** 75
[36] Zhang W, Li M, Jia M, Fan Y, Zhang Y, Tian Z, Li X, Liu Y, Yang D, Song H and Cabot A 2024 *J. Eur. Ceram. Soc.* **44** 5088
[37] Cao R, Zhu Z, Li X J, Hu X and Song H 2019 *Appl. Phys. A* **125** 126
[38] Cao R, Liu X, Tian Z, Zhang Y, Li X J and Song H 2022 *Appl. Phys. A* **128** 1130
[39] Xu Z, Hu L, Ying P, Zhao X and Zhu T 2015 *Acta Materialia* **84** 385
[40] Xiong C, Shi F, Wang H, Cai J, Zhao S, Tan X, Hu H, Liu G, Noudem J G and Jiang J 2021 *ACS Appl. Mater. Interfaces* **13** 15429
[41] Zhang W, Liu X, Tian Z, Zhang Y, Li X J and Song H 2023 *J. Electron. Mater.* **52** 6682
[42] Zhang W, Li M, Zhang Y, Tian Z, Li X J and Song H 2024 *J. Alloys Compd.* **993** 174672
[43] Shen J J, Zhu T J, Zhao X B, Zhang S N, Yang S H and Yin Z Z 2010 *Energy Environm. Sci.* **3** 1519
[44] Pei J, Cai B, Zhuang H L and Li J F 2020 *Nat. Sci. Rev.* **7** 1856
[45] Huang H, Li J, Chen S, Zhang Z, Yan Y, Su X and Tang X 2020 *J. Solid State Chem.* **288** 121433
[46] Bies W, Radtke R, Ehrenreich H and Runge E 2002 *Phys. Rev. B* **65** 085208
[47] Yang S, Ming H, Li D, Chen T, Li S, Zhang J, Xin H and Qin X 2023 *Chem. Eng. J.* **455** 140923
[48] Li S, Wang L, Ma D, Jiang Y, Zhang J and Guo K 2024 *ACS Appl. Mater. Interfaces* **16** 3586
[49] Ahmad A, Zhu B, Wang Z, Gui Z, Wang W, Wang T, Yu Y, Huang L and He J 2024 *Energy Environm. Sci.* **17** 695
[50] Liu X, Cao R, Zhang Y, Tian Z, Li X J and Song H 2022 *J. Alloys Compd.* **899** 163296
[51] Mehta R J, Zhang Y, Karthik C, Singh B, Siegel R W, Borca-Tasciuc T and Ramanath G 2012 *Nat. Mater.* **11** 233
[52] Li J, Tan Q, Li J F, Liu D W, Li F, Li Z Y, Zou M and Wang K 2013 *Adv. Funct. Mater.* **23** 4317
[53] Hu L, Zhu T, Liu X and Zhao X 2014 *Adv. Funct. Mater.* **24** 5211
[54] Kim S I, Lee K H, Mun H A, Kim H S, Hwang S W, Roh J W, Yang D J, Shin W H, Li X S and Lee Y H 2015 *Science* **348** 109
[55] Hong M, Chen Z G, Yang L and Zou J 2016 *Nano Energy* **20** 144
[56] Yu Y, He D S, Zhang S, Cojocaru-Mirédin O, Schwarz T, Stoffers A, Wang X Y, Zheng S, Zhu B and Scheu C 2017 *Nano Energy* **37** 203
[57] Deng R, Su X, Zheng Z, Liu W, Yan Y, Zhang Q, Dravid V P, Uher C, Kanatzidis M G and Tang X 2018 *Sci. Adv.* **4** eaar5606
[58] Liu Y, Zhang Y, Ortega S, Ibáñez M, Lim K H, Grau-Carbonell A, Martí-Sánchez S, Ng K M, Arbiol J and Kovalenko M V 2018 *Nano Lett.* **18** 2557
[59] Pan Y, Qiu Y, Witting I, Zhang L, Fu C, Li J W, Huang Y, Sun F H, He J and Snyder G J 2019 *Energy Environm. Sci.* **12** 624
[60] Li C, Ma S, Wei P, Zhu W, Nie X, Sang X, Sun Z, Zhang Q and Zhao W 2020 *Energy Environm. Sci.* **13** 535
[61] Zhuang H L, Pei J, Cai B, Dong J, Hu H, Sun F H, Pan Y, Snyder G J and Li J F 2021 *Adv. Funct. Mater.* **31** 2009681
[62] Wang X, Cheng J, Yin L, Zhang Z, Wang X, Sui J, Liu X, Mao J, Cao F and Zhang Q 2022 *Adv. Funct. Mater.s* **32** 2200307
[63] Sun Y, Wu H, Dong X, Xie L, Liu Z, Liu R, Zhang Q, Cai W, Guo F and Sui J 2023 *Adv. Funct. Mater.* **33** 2301423
[64] Shi Y C, Yang J, Wang Y, Li Z G, Zhong T Y, Ge Z H, Feng J and He J 2024 *Energy Environm. Sci.* **17** 2326
[65] Zhuang H L, Cai B, Pan Y, Su B, Jiang Y, Pei J, Liu F, Hu H, Yu J and Li J W 2024 *Nat. Sci. Rev.* **11** nwae329
[66] Xu S, Horta S, Lawal A, Maji K, Lorion M and Ibáñez M 2025 *Science* **387** 845